The current issue and full text archive of this journal is available at
www.emeraldinsight.com/0961-5539.htm



# Using localized wall discharge to control the fluid flow and heat transfer for the flow over a backward facing step

Suhil Kiwan
*Mechanical Engineering Department,*
*Jordan University of Science and Technology, Irbid, Jordan*

Received 14 September 2006
Revised 25 May 2007
Accepted 7 June 2007

## Abstract

**Purpose** – Studying the effect of localized wall discharge on the fluid flow and heat transfer for a flow over backward facing step is the main purpose of this paper. Jet is used to control the reattachment length which controls the fluid flow and heat transfer downstream the step. Several parameters are to be investigated: geometric; expansion ratio, location of the jet, and jet angle flow; Reynolds number, jet velocity.

**Design/methodology/approach** – Numerical simulation using both the standard $K-\varepsilon$ and renormalized group turbulence theory (RNG) $K-\varepsilon$ models are used to model flow in the computational domain. The energy equation is also used to model the heat transfer characteristics of the flow. The model equations are solved numerically using a finite volume code.

**Findings** – It is found that the presence of the wall jet at a proper location can significantly influence the flow and heat characteristics of the problem. Furthermore, varying the ratio of the jet velocity to the main stream velocity could play an important role in controlling the size of the circulating bubble and, therefore, the fluid and heat transfer characteristics of the flow, whereas, the expansion ratio has less influence. It is also found that increasing Reynolds number increases the value of maximum heat transfer but has less influence on either its location or the reattachment length.

**Research limitations/implications** – The range of the Reynolds number considered in this research covers only the turbulent regime. The research does not cover laminar flows. The results and conclusions cover only three values of expansion ratios. Namely (expansion ratio (ER) = 1.67, 1.8 and 2). Conclusions should not be read beyond these values of ER.

**Practical implications** – This work gives designers of similar flows a new method of controlling the fluid flow and heat transfer by varying jet angle.

**Originality/value** – This work has not been done before and it can initiate additional research projects as investigating the effect of applying wall jets in combustors.

**Keywords** Heat transfer, Flow, Simulation, Jets

**Paper type** Research paper

## Nomenclature

$C$ = channel height at inlet
$C_f$ = skin friction coefficient ($2\tau_w/\rho U_\infty^2$)
$C_p$ = pressure coefficient ($(P-P_\infty)/0.5\rho U_\infty^2$)
$c_p$ = specific heat at constant pressure
ER = expansion ratio ($(C+H)/C$)
$h$ = heat transfer coefficient ($q''_w/(T_w-T_\infty)$)
$h_{max}$ = maximum heat transfer coefficient along step wall

The author would like to acknowledge both the engineering research center at King Saud University and the Jordan University of Science and Technology for their support to the this work.

International Journal of Numerical Methods for Heat & Fluid Flow
Vol. 18 No. 6, 2008
pp. 745-765

0961-5539
DOI 10.1108/09615530810885551

$H$ = step height
$K$ = turbulent kinetic energy
$N_J$ = ratio of jet velocity to incoming free stream velocity ($V_J/U_\infty$)
$P$ = Pressure
$Pr$ = Prandtl number ($\nu/\alpha$)
$Re_H$ = Reynolds number based on step height ($U_\infty H/\nu$)
$St$ = Stanton number ($h/\rho U_\infty c_p$)
$T$ = temperature
$T_\infty$ = incoming free stream temperature
$q''$ = heat flux
$U$ = time averaged axial velocity
$U_\infty$ = incoming free stream velocity
$V$ = time averaged transverse velocity
$w$ = width of jet slot
$x$ = axial distance
$X_r$ = reattachment length normalized by step height ($x_r/H$)
$X_m$ = location of $h_{max}$ ($x_m/H$)
$X_J$ = location of jet normalized by step height ($x_J/H$)
$y$ = transverse distance measured from step corner

*Subscript*
max = maximum
o = reference case
w = wall
$\infty$ = free stream conditions

*Greek symbols*
$\alpha$ = thermal diffusivity
$\alpha_{eff}$ = effective thermal diffusivity
$\delta$ = boundary layer thickness
$\varepsilon$ = turbulent energy dissipation
$\mu$ = dynamic viscosity
$\mu_{eff}$ = effective viscosity calculated from equation (12)
$\mu_T$ = eddy viscosity
$\nu$ = kinematics viscosity
$\theta$ = jet angle as shown in Figure 1
$\rho$ = density

## 1. Introduction

Separation and reattachment of flows occur in many practical engineering applications. In particular, the flow over a backward-facing-step situation appears in many thermal engineering applications where heating and cooling are required. These applications include cooling systems for electronic components, combustion chambers, pipes and ducts of air conditioning systems, chemical processes, high-performance heat exchangers, and in cooling passages of turbine blades. The existence of flow separation and subsequent reattachment greatly influence the mechanism of heat transfer. Therefore, it is essential to understand the basic mechanism of heat transfer in such situations in order to control the heat transfer.

The sudden expansion formed by a backward facing step received the attention of investigators for many years. Various studies have been conducted aiming at controlling the location of the reattachment point. These studies used active and passive control mechanisms. Works on active control mechanisms included the use of electromagnetic actuators (Inaoka *et al.*, 2004), mass injection (Vakili and Gauthier, 1994) or bleeding (Chyu *et al.*, 1995), vortex generators (Barter and Dolling, 1995), acoustic excitation (Roos and Kegelman, 1986; Joslin *et al.*, 1995), imposed wall heat flow (Kral and Fasel, 1994), and moving fences or flaps (Nelson *et al.*, 1990; Garsul *et al.*, 1995). Passive control methods incorporated fixed attachments to modify the flow for a given range of operating conditions. Such methods include the use of surface ripplets (Debisschop and Nieuwstat, 1996), cavities (Zhang, 1995), porous surfaces (Hanna, 1995), inserting stationary cylinders (Suzuki *et al.*, 1991) and rotating cylinders (Abu-Hijleh, 2000). A thorough review of earlier work in the area of boundary layer control was given by Gad-el-Hak and Bushnell (1991). Most of the above studies investigated the flow aspect but not the heat transfer aspect of the problems. Oyakawa *et al.* (1986) studied the effect of inserting different geometric shapes in rectangular

ducts on the heat transfer characteristics. Also, Oyakawa *et al.* (1995) studied experimentally the effect of using jet discharge on the reattachment heat transfer in the region downstream of a backward facing step.

Unlike turbulent models used to predict the hydrodynamics of flows, the models used to predict the heat transfer of turbulent flow are of less success. The usual practice, in many cases, is to tune up model constants in a way that the predictions are close to the experimental results. A considerable research carried out to solve the hydrodynamic and heat transfer characteristics of complex flows involving separation and reattachments. Conventional turbulence modeling methods such as the Reynolds Averaged Navier Stokes (RANS) approach have been the main approach used by many researchers. RANS approaches using standard turbulent models have not been successful in predicting all flow and heat transfer features in complex flows. Avancha and Pletcher (2002) used large-eddy-simulations (LES) technique to study the fluid flow and heat transfer over a backward step heated with a uniform heat flux. They found that the viscous sub-layer plays a critical role in controlling the heat transfer rate. They also found a close similarity between the Stanton number and the fluctuating skin friction profiles. Their results agreed with the experiment of Vogel and Eaton (1985) in that the Stanton number attains its maximum upstream the reattachment point. However, using LES requires high speed and large capacity computers.

Most of the computational work was aimed at reproducing experimental data of a certain flow. It is good to have a simple model that is able to predict correctly all flows. But, if these models are not able to quantitatively predict these data then it would be helpful to inspect their strength in predicting relative effects of changing parameters. That is, if a certain model underestimates the maximum value of Stanton number produced experimentally at all Reynolds numbers, then, it is not necessarily that the ratio of maximum value of Stanton number at any Reynolds number when normalized by a reference case produced by the same model under-predicts the experimental results when normalized in the same manner.

The present investigation examines the effect of localized wall jet on the flow and heat transfer characteristics of a flow over backward facing step for different jet velocities, jet location, step heights and Reynolds numbers. Using jet as a controller has the advantage of active controllers in that it offers better control over a wide range of operating conditions and the simplicity of passive controllers in that its relative ease of use in practical situations. The standard and the renormalized group turbulence theory (RNG) models are used in this study. Both models were previously tested in similar cases. The standard $K-\varepsilon$ model is reported to give results deviates from experimental data (Abe *et al.*, 1995; Kiwan, 1995), whereas, the RNG model is reported to give good predictions to similar problems (Abu-Hijleh, 2000).

## 2. Problem formulation

Figure 1 shows a fluid moving over a backward facing step at a velocity $U_\infty$ and a temperature $T_\infty$. Slot jet is located on the wall opposing to the step wall. All walls except the step wall are assumed to be insulated. The step wall is heated with constant heat flux. The induced motion of the fluid is assumed to be turbulent, steady, 2D flow. All thermo-physical properties are considered to be constant. The governing equations along with the proper boundary conditions are solved numerically using a finite volume solver.

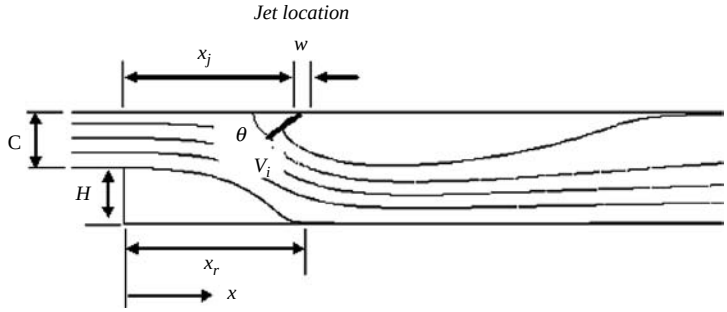


| Case | J0 | J1 | J2 | J3 | J4 | J5 | J7 |
|---|---|---|---|---|---|---|---|
| Jet Location, $X_J=x_J/H$ | No jet | 1.1 | 2.1 | 3.1 | 4.1 | 5.1 | 7.1 |

**Note:** Reproduced from the only available original

**Figure 1.**
Schematic diagram for the problem under consideration

The Reynolds-averaged continuity, momentum and energy equations required to completely describe turbulent flow of a viscous incompressible fluid with constant properties are:

$$\frac{\partial U}{\partial x}+\frac{\partial V}{\partial y}=0 \tag{1}$$

$$\rho U\frac{\partial U}{\partial x}+\rho V\frac{\partial U}{\partial y}=-\frac{\partial P}{\partial x}+\frac{\partial}{\partial x}\left[(\mu+\mu_{\mathrm{T}})\frac{\partial U}{\partial x}\right]+\frac{\partial}{\partial y}\left[(\mu+\mu_{\mathrm{T}})\frac{\partial U}{\partial y}\right] \tag{2}$$

$$\rho U\frac{\partial V}{\partial x}+\rho V\frac{\partial V}{\partial y}=-\frac{\partial P}{\partial y}+\frac{\partial}{\partial x}\left[(\mu+\mu_{\mathrm{T}})\frac{\partial V}{\partial x}\right]+\frac{\partial}{\partial y}\left[(\mu+\mu_{\mathrm{T}})\frac{\partial V}{\partial y}\right] \tag{3}$$

$$\left(U\frac{\partial T}{\partial x}+V\frac{\partial T}{\partial y}\right)=\frac{\partial}{\partial x}\left[\alpha_{\mathrm{eff}}\frac{\partial T}{\partial x}\right]+\frac{\partial}{\partial y}\left[\alpha_{\mathrm{eff}}\frac{\partial T}{\partial y}\right] \tag{4}$$

The effect of body forces is neglected in equation (1). The eddy viscosity is given by:

$$\mu_{\mathrm{T}}=C_{\mu}\rho\frac{K^2}{\varepsilon} \tag{5}$$

where $C_{\mu}$ is constant. $K$ and $\varepsilon$ are calculated from the following equations (Mohammadi and Pironnean, 1993):

$$\begin{aligned}\rho U\frac{\partial K}{\partial x}+\rho V\frac{\partial K}{\partial y}=&\frac{\partial}{\partial x}\left[\left(\mu+\frac{\mu_{\mathrm{T}}}{\sigma_{\mathrm{K}}}\right)\frac{\partial K}{\partial x}\right]+\frac{\partial}{\partial y}\left[\left(\mu+\frac{\mu_{\mathrm{T}}}{\sigma_{\mathrm{K}}}\right)\frac{\partial K}{\partial y}\right]-\rho\varepsilon\\&+\mu_{\mathrm{T}}\left[2\left(\frac{\partial U}{\partial x}\right)^2+2\left(\frac{\partial V}{\partial y}\right)^2+\left(\frac{\partial U}{\partial y}+\frac{\partial V}{\partial x}\right)^2\right]\end{aligned} \tag{6}$$

$$\rho U\frac{\partial \varepsilon}{\partial x}+\rho V\frac{\partial \varepsilon}{\partial y}=\frac{\partial}{\partial x}\left[\left(\mu+\frac{\mu_{\mathrm{T}}}{\sigma_{\mathrm{K}}}\right)\frac{\partial \varepsilon}{\partial x}\right]+\frac{\partial}{\partial y}\left[\left(\mu+\frac{\mu_{\mathrm{T}}}{\sigma_{\mathrm{K}}}\right)\frac{\partial \varepsilon}{\partial y}\right]-C_2\rho\frac{\varepsilon^2}{K}+C_1\mu_{\mathrm{T}}\frac{\varepsilon}{K}\left[2\left(\frac{\partial U}{\partial x}\right)^2+2\left(\frac{\partial V}{\partial y}\right)^2+\left(\frac{\partial U}{\partial y}+\frac{\partial V}{\partial x}\right)^2\right] \tag{7}$$

Equations (2)-(7) forms the standard $K-\varepsilon$ model where $C_1, C_2, C_\mu, \sigma_{\mathrm{K}},$ and $\sigma_\varepsilon$ are constants having the values, 1.44, 1.92, 0.09, 1.00, and 1.3, respectively. Yakhot and Orszag (1986) introduced a modified $K-\varepsilon$ model based on the RNG. In the RNG model, $C_1$ in equation (7) is not constant and is calculated as (Mohammadi and Pironnean, 1993):

$$C_1=C_0-\frac{\eta(1-\eta/\eta_0)}{1+\beta\eta^3} \tag{8}$$

$$\eta=\frac{\sqrt{G}K}{\varepsilon} \tag{9}$$

$$G=\left[2\left(\frac{\partial U}{\partial x}\right)^2+2\left(\frac{\partial V}{\partial y}\right)^2+\left(\frac{\partial U}{\partial y}+\frac{\partial V}{\partial x}\right)^2\right] \tag{10}$$

The RNG model introduces three additional constants, $C_0, \beta,$ and $\eta_0$. The values of the constants for the RNG model used in this study are:

$$C_2=1.68, C_\mu=0.0845, C_0=1.42, \sigma_{\mathrm{K}}=0.7179, \sigma_\varepsilon=0.7179, \beta=0.012, \text{ and } \eta_0=4.38$$

On the other hand, the value of the effective thermal diffusivity, $\alpha_{\mathrm{eff}}$ is calculated for the standard $K-\varepsilon$ model as:

$$\alpha_{\mathrm{eff}}=(\alpha+\alpha_{\mathrm{T}})=\alpha+\frac{\mu_{\mathrm{T}}}{\rho Pr_{\mathrm{t}}} \tag{11}$$

And for the RNG model as:

$$\alpha_{\mathrm{eff}}=\frac{\alpha\mu_{\mathrm{eff}}}{\rho} \tag{12}$$

where $\mu_{\mathrm{eff}}$ is calculated from the equation (Choudhury, 1993):

$$\left|\frac{\alpha-1.3929}{1-1.3929}\right|^{0.6321}\left|\frac{\alpha+2.3929}{1+2.3929}\right|^{0.3679}=\frac{\mu}{\mu_{\mathrm{eff}}} \tag{13}$$

Several flow and geometric parameters control the flow and heat transfer of the problem under consideration. These include the Reynolds number of the inlet flow, $Re_{\mathrm{H}}$, jet velocity ratio, $V_{\mathrm{J}}/U_\infty$, expansion ratio, jet location, jet angle, and width of jet slot, $w$. In this study, the expansion ratio is changed by changing the height of the channel at inlet, $C$. Both the step height and the ratio of the width of the jet slot to the step height are fixed. The ratio of the jet slot width to the step height is fixed to a value of 0.073 as given by Oyakawa *et al.* (1995).

At the flow inlet and jet inlet, the velocity, temperature, turbulence kinetic energy, and dissipation are specified. At the flow inlet, the values of velocity, turbulence kinetic energy, and dissipation are specified from a previous run in a straight channel of similar width and $Re_H$ such that $\delta/H = 1.1$. Zero gage pressure is specified at the exit. Constant heat flux is specified at step wall. All other walls are assumed insulated.

## 3. Numerical solution

The governing equations along with the proper boundary conditions are solved over a simple 2D mesh using a finite volume solver (Fluent, 2001). The pressure field is calculated using the simple algorithm. The hybrid-differencing scheme is used to difference the convective terms. The iterative solution is considered to have converged when the maximum of the normalized absolute residual across all nodes is less than $10^{-6}$.

The computational domain downstream the step is divided into four segments as shown in Figure 2. This simplifies the control the mesh and to use fine uniform mesh wherever is expected to have high-gradients downstream the step. The first segment is the region between the step and the location of the jet. The second segment is the zone where the jet is located. The third segment is between the jet and $x/H = 20$, and the last segment from $x/H = 20$ to the end of the computational domain. Several runs are carried out to locate the end of the computational domain. It is located such that the flow leaving the computational domain is fully developed. It is found that locating the end of the computational at $x/H = 120$ satisfies this requirement for both models and all jet locations used in this study. Therefore, the computational domain is: $-2.0 \leq x/H \leq 120$. A uniform mesh is used in the first three segments downstream the step. It should be

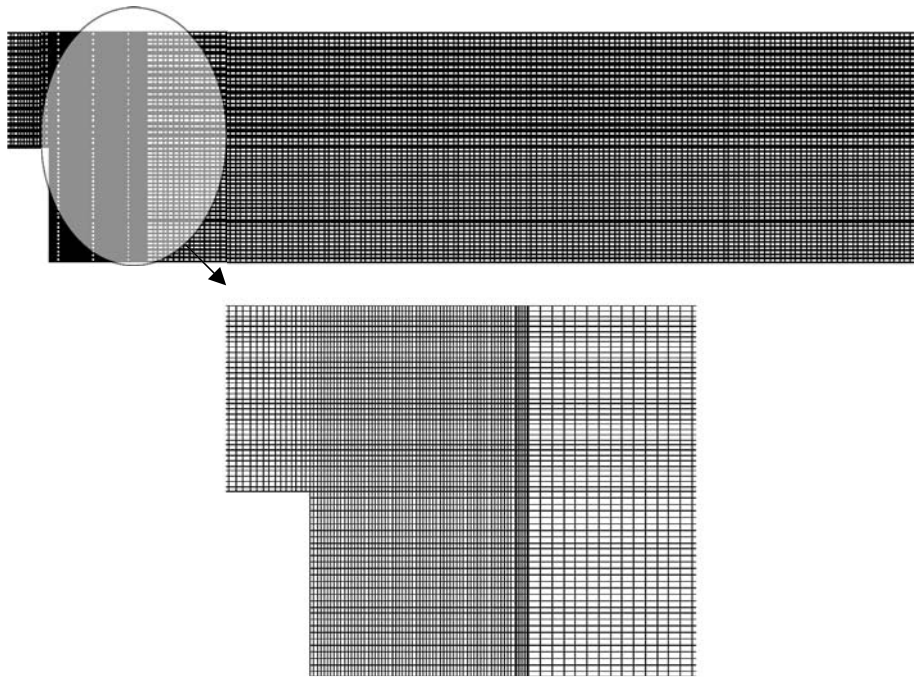

**Figure 2.**
The grid of the computational domain

noted that use of wall functions require that the first mesh point adjacent to the wall to be located in the logarithmic layer of the turbulent boundary layer ($y^+ \approx 30 - 60$). This requirement reduces the number of grid points required to solve the flow across the turbulent boundary layer. Therefore, a uniform mesh is used across the channel.

Several mesh sizes are tested to obtain a grid independent solution. The solution is obtained for each mesh and compared with the result obtained from previous mesh until we arrive at a mesh where the solution changes within 1 per cent. The heat transfer coefficient, $h$, and the pressure coefficient, $C_p$ at the heated wall downward the step are used to test grid independence. Figure 3 shows a comparison between the distribution of the:

- heat transfer coefficient; and
- pressure coefficient along the step wall using two different grids for the case of no jet.

The change in the heat transfer coefficient and pressure coefficient between the solutions obtained from a 30,000-node-mesh and a 40,000-node-mesh using the standard $K - \varepsilon$ model is less than 1 per cent. Figure 4(a) shows that using 30,000 or 40,000 or 50,000 nodal-mesh for J7 and $N_J = 2$ case satisfies the grid independent solution criterion based on heat transfer coefficient. On the other hand, Figure 4(b) shows that using a 30,000-nodal mesh is not enough to satisfy the pressure coefficient criterion, while, the 40,000 or 50,000-nodal-mesh satisfies both criteria, therefore, the 50,000-nodal mesh is used through out the present work.

To verify the numerical code used in the present work, the results of the present code are tested and compared with the results obtained by Vogel and Eaton (1985). Table I shows a comparison between the present code results using the standard and the RNG $K - \varepsilon$ models and the experimental results for the flow over a backward facing step of Vogel and Eaton (1985). It is clear from these tables that the RNG model shows a good agreement with the experimental data, while, the standard $K - \varepsilon$ model under-predicts the reattachment length by 20 per cent. In general, both models captured the trend of the distribution of the Stanton number over the heated wall.

## 4. Results and discussions

The results presented in the next three sections are limited to perpendicular jets, whereas, the effect of varying jet angle is considered in Section 4.5.

### *4.1 Effect of jet location*

The effect of jet location on the reattachment length (i.e. circulating bubble), the location of $h_{max}$ and on the distribution of the pressure and heat transfer coefficients are presented here. Figure 5 shows the streamlines for different jet locations when $N_J = 2$ using the Standard $K - \varepsilon$ model. These streamlines show the general flow features for different jet locations. The incoming flow separates at the edge of the flow due to the sudden expansion. Two primary recirculation regions develop; one adjacent to the step after the boundary separation and shear layer impingement on to the bottom wall. The second recirculation region is behind the jet on the opposing wall. It is clear from this figure that the size of the circulating bubble adjacent to the step is large in the absent of jet and it is significantly decreased as the jet is applied and moved closer to the step wall. It is anticipated that, the presence of the recirculating bubble

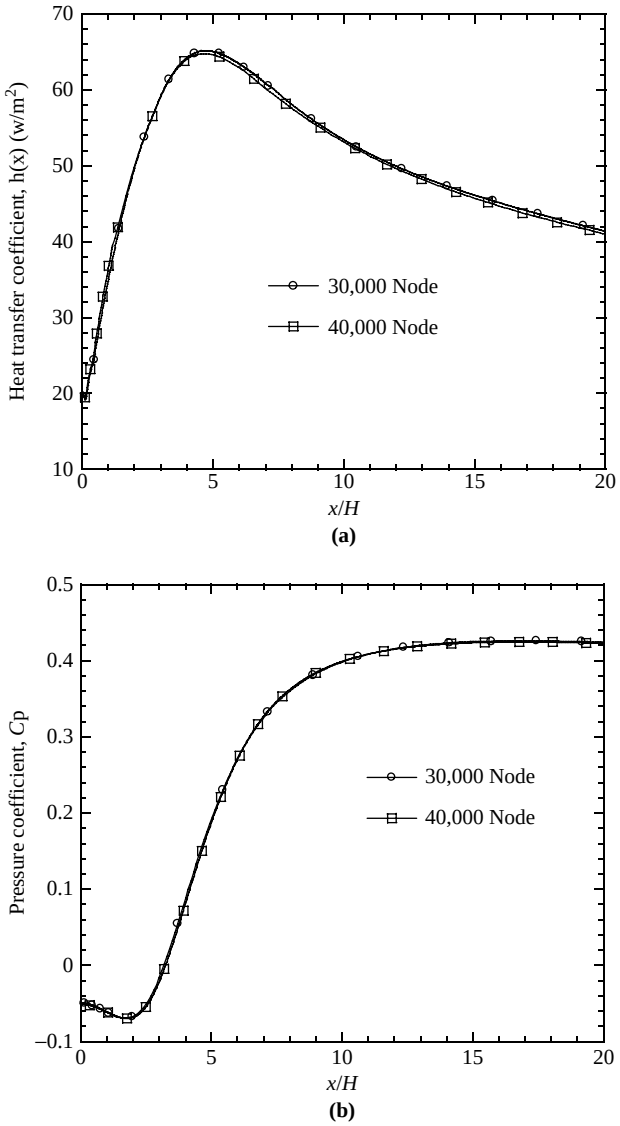


**Figure 3.**
Effect of grid points on the numerical solution: (a) heat transfer coefficient; (b) pressure coefficient at step wall for no jet case

behind the jet to greatly affect the flow characteristics along the step wall because the flow will accelerate when it passes through the region between the two bubbles and, therefore, the circulating bubble close to the step will be squeezed. Similar results are obtained using the RNG model.

Figure 6(a) shows the distribution of the heat transfer coefficient and pressure coefficient for different jet location using the standard $K - \varepsilon$ model. It is clear from this figure that the value of $h_{\max}$ when jet is applied, in the locations considered here, is

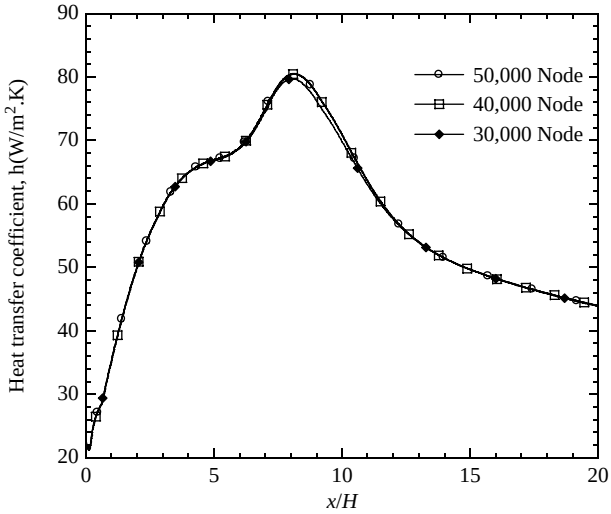


**Notes:** ER = 2.0; $N_J$ = 2.0

**Figure 4.**
Effect of grid points on the numerical solution: (a) heat transfer coefficient; (b) pressure coefficient at step wall when jet is at $x/H = 7.1$

| Model | $X_m$ | $St$ | $X_r$ | Percentage of error in $X_r$ | Percentage of error in $St$ | Percentage of error in $X_m$ |
|---|---|---|---|---|---|---|
| RNG | 5.48 | $3.3 \times 10^{-3}$ | 6.43 | −3.6 | −3.6 | −6.3 |
| $K - \varepsilon$ | 4.52 | $3.4 \times 10^{-3}$ | 5.25 | −21.2 | 0.8 | −22.8 |
| Experiment | 5.86 | $3.4 \times 10^{-3}$ | 6.67 | – | – | – |

**Table I.**
Comparison between the numerical results and the experimental results of Vogel and Eaton (1985)

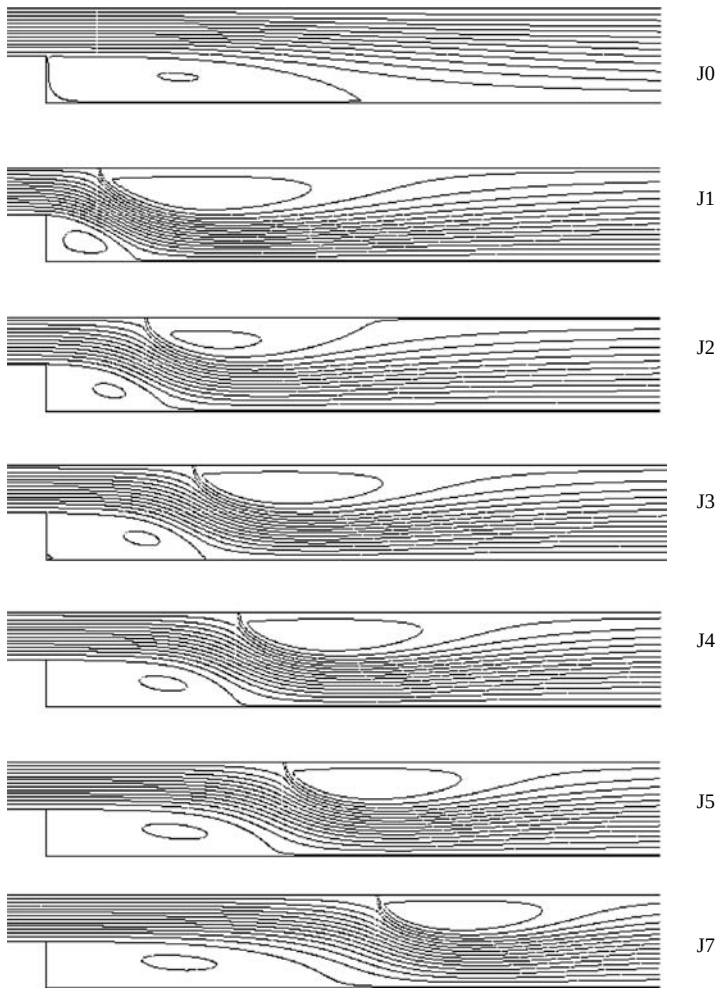


**Figure 5.**
Streamlines for different jet locations obtained using the RNG $k - \varepsilon$ model

**Notes:** ER = 2; $N_J$ = 2; $Re_H = 3.8 \times 10^4$; Reproduced from the only available original

higher than that when the jet is absent. The presence of two bubbles opposing to each other creates a jet effect to the main stream (flow between the two bubbles). This increases the curvature of the streamlines of the shear layer and squeezes the bubble close to the step wall. Consequently, both the intensity of the flow inside the recirculation region close to the step and the heat transfer from the heated wall increases. As the jet moves downstream the step the interaction between the two bubbles decreases. This decrease the size and the intensity of the flow inside the recirculation region close to step, and, consequently, the value of $h_{max}$.

On the other hand, the location of $h_{max}$ and $X_r$ is greatly influenced by the presence of the jet. Figure 6(b) shows that when jet is absent the pressure coefficient decreases to a minimum value near $x/H = 2.5$ and then increases to its maximum value near the

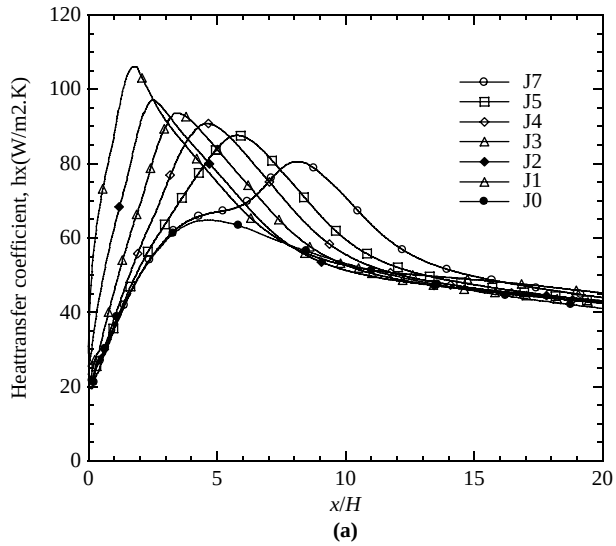


**Notes:** ER = 2; $N_J$ = 2; $Re_H = 3.8\times10^4$

**Figure 6.**
The distribution of the: (a) heat transfer coefficient; and (b) pressure coefficient for different jet locations

reattachment point. When the jet is applied, the presence of the circulating bubble on the jet wall accelerates the main flow which leads to drop the pressure and therefore an extra maximum and minimum values of $C_p$ appears. The first maximum value of $C_p$ appears at the reattachment point at the step wall and the second maximum value coincides with the reattachment point of the circulating bubble formed by the jet. It is also clear from this figure that the value of $C_p$ max increases as the jet moves downstream. This agrees with the experimental findings of Oyakawa *et al.* (1995).

It is very difficult to decide on the degree of agreement between the computational results and the experimental results when experimental results lack important information needed for computational simulation. Therefore, it may be better to present the results on relative predications bases within the used model. That is, variation of $h_{max}$, $X_m$ and $X_r$ will be normalized by $h_{max0}$, $X_{m0}$ and $X_{r0}$, respectively. The values of $h_{max0}$, $X_{m0}$ and $X_{r0}$ are the obtained values when jet is absent. The ratio of $h_{max}/h_{max0}$ is shown in Figure 7(a). This figure indicates that there is an agreement of the effect of jet location on the value of $h_{max}$ between the data obtained experimentally and numerically at almost all jet locations. This figure also indicates that as the jet moves away from the step wall the ratio of $h_{max}/h_{max0}$ goes toward one. Figure 7(b) shows that this agreement is not the same when it comes to the predictions of the location of $h_{max}$. However, the ratio of $X_r/X_{r0}$ obtained by the Standard $K - \varepsilon$ model is closer to the experimental predictions than that obtained by the RNG model as evidence by Figure 7(c).

*4.2 Effect of jet velocity*

Four different values of jet velocity ratios, $N_J$ are used in order to study the effect of varying jet velocity ratio on $h_{max}$, $X_m$ and $X_r$. Namely, $N_J = 1.0$, 1.5, 1.8 and 2.0. It should be mentioned that wherever it is necessary the values of the following parameters are fixed: ER = 2.0, $Re_H = 38 \times 10^3$, $N_J = 2.0$. This is applied to this section and the following two sections.

Figure 8 shows the streamlines for this case where the results are obtained using the RNG model and jet is located at $x/H = 3.1$. As shown in Figure 8, increasing the jet velocity results in increasing the size of the recirculation region behind the jet and, therefore, squeezing the recirculation region behind the step. Thus, as it is shown in Figure 9(a), increasing the jet velocity results in increasing the value of $h_{max}$ and decreasing the value of $X_m$. Figure 9(b) shows that decreasing $N_J$ increases the value of $X_r$ and value of the new $C_p$ minimum. It should be mentioned that similar trends are obtained at different jet locations and using the standard $K - \varepsilon$ model.

*4.3 Effect of Reynolds number,* $Re_H$

Three different values Reynolds numbers are used to examine the effect of varying Reynolds number on $h_{max}$, $X_m$ and $X_r$. Namely, $Re_H = 25 \times 10^3$, $38 \times 10^3$ and $51 \times 10^3$. Figure 10 shows that increasing $Re_H$ almost has no effect on either $X_r$ or $X_m$. On the other hand, it shows that increasing $Re_H$ increases the ratio $h_{max}/h_{max0}$.

*4.4 Effect of expansion ratio, ER*

To examine the effect of changing the expansion ratio, ER on $h_{max}$, $X_m$ and $X_r$, three different values ER are used. These values are selected to insure that the jet flow interacted with the main stream and the shear layer. Namely, ER = 2, ER = 1.8, and ER = 1.67. The variation of ER is achieved by changing the height of the inlet channel, $C$. Table II shows the results obtained at three different jet locations. The results show no significant change in the reattachment length, or $h_{max}$ and $X_m$ among the expansion ratios considered here. Increasing the expansion ratio has two counter effects on the flow: first, as the expansion ratio increases, the distance between the wall jet and the heated wall increases. and, thus, reduces the jet effect of the main stream which results in reducing the value of $h_{max}$, and increasing the value of $X_r$.

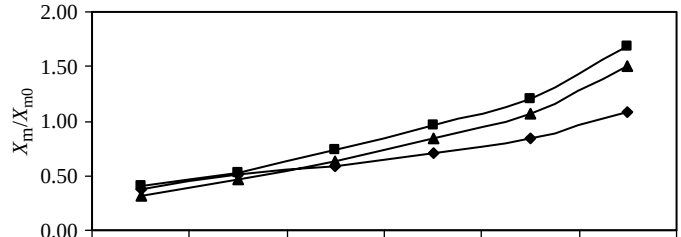


| | J1 | J2 | J3 | J4 | J5 | J7 |
|---|---|---|---|---|---|---|
| Exp.[8] | 0.38 | 0.51 | 0.59 | 0.71 | 0.84 | 1.08 |
| Stand. | 0.40 | 0.53 | 0.73 | 0.97 | 1.21 | 1.69 |
| RNG | 0.32 | 0.47 | 0.63 | 0.84 | 1.07 | 1.50 |

**(a)**

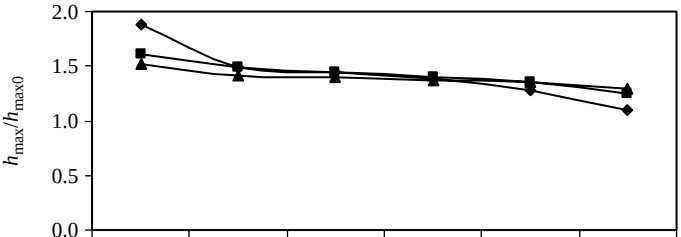


| | J1 | J2 | J3 | J4 | J5 | J7 |
|---|---|---|---|---|---|---|
| Exp.[8] | 1.89 | 1.49 | 1.45 | 1.38 | 1.28 | 1.10 |
| Stand. | 1.62 | 1.50 | 1.44 | 1.40 | 1.36 | 1.25 |
| RNG | 1.51 | 1.42 | 1.40 | 1.37 | 1.35 | 1.29 |

**(b)**

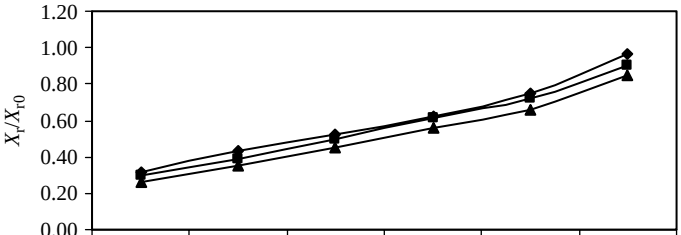


| | J1 | J2 | J3 | J4 | J5 | J7 |
|---|---|---|---|---|---|---|
| Exp.[8] | 0.32 | 0.43 | 0.53 | 0.63 | 0.75 | 0.97 |
| Stand. | 0.30 | 0.39 | 0.50 | 0.62 | 0.73 | 0.90 |
| RNG | 0.26 | 0.35 | 0.46 | 0.56 | 0.66 | 0.84 |

**(c)**

**Notes:** ER = 2; $N_J$ = 2; $Re_H = 3.8\times10^4$

**Figure 7.**
The variation of: (a) ratio of $h_{max}/h_{max0}$, (b) $X_m/X_{m0}$; and (c) reattachment length ratio $X_r/X_{r0}$ with jet location

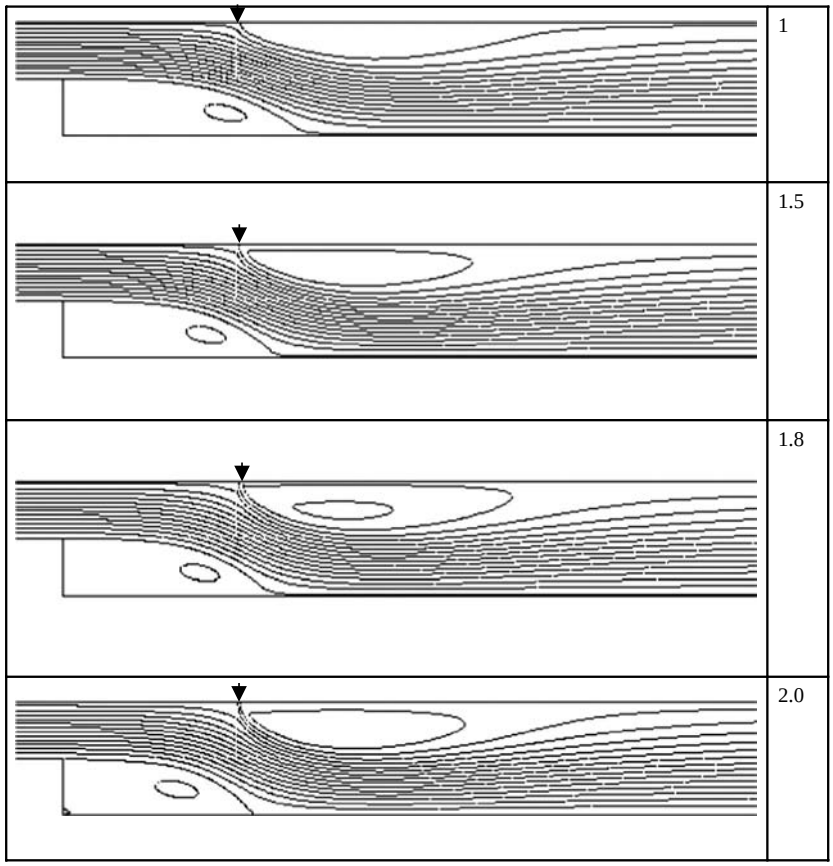


**Figure 8.**
Streamlines for different jet velocity ratios

**Notes:** The arrow indicates the location of the jet ($X_J$ = 3.1; ER = 2; $Re_H = 3.8\times10^4$) ; Reproduced from the only available original

On the other side, increasing the expansion ratio results in reducing the pressure downstream the step and, thus, the flow of the wall jet penetrates deeper into the main stream. This result in increasing the size of the bubble behind the wall jet and, therefore, squeezing the recirculating region close to the step which increases the value of $h_{max}$, and decreases the value of $X_r$. The net effect of increasing the expansion ratio depends on which effect dominates. It is clear that the two effects, in the range of flow variables and expansion ratios considered in this study, are of the same order of magnitude. Therefore, changing the expansion ratio shows a little influence on the flow and heat transfer characteristics.

*4.5 Effect of jet angle, $\theta$*

Figure 11 shows the variation of the skin friction coefficient at the step wall at different jet angles. It is clear from this figure that the jet angle plays an important role in deciding the location of the reattachment length. As the jet angle increases the reattachment length increases until $\theta$ reaches 140° where a further increase does not

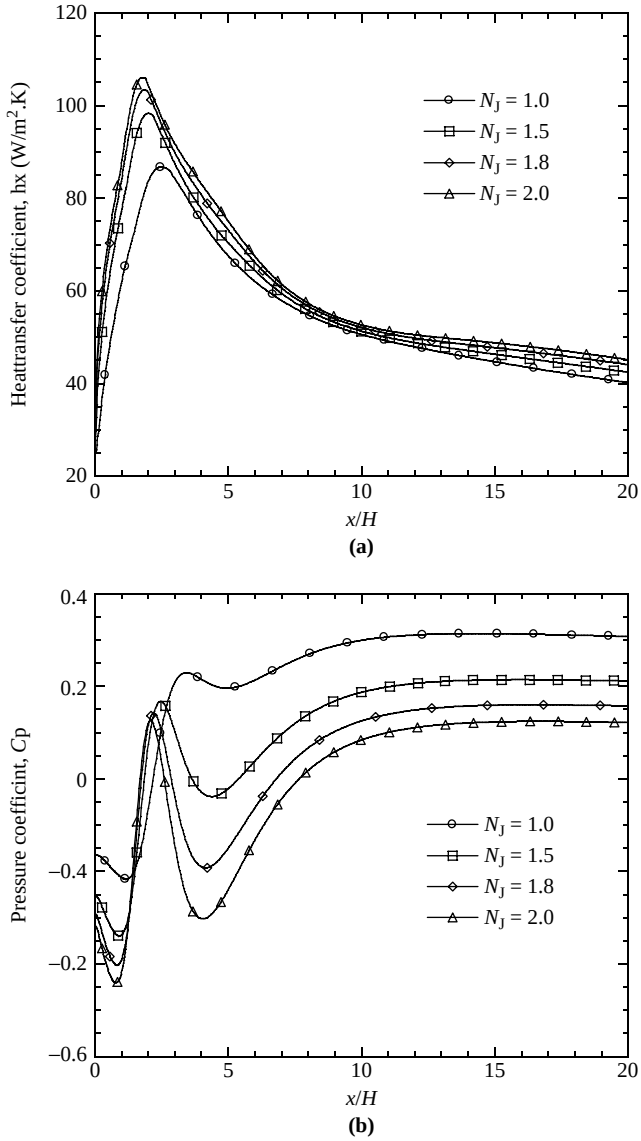


**Notes:** ER = 2; $X_J$ = 1.1; $Re_H = 3.8\times10^4$

**Figure 9.**
The distribution of the: (a) heat transfer coefficient; and (b) pressure coefficient for different jet velocity ratios

have a significant influence on the reattachment length. This is due to the fact that the size of the circulating bubble formed behind the jet decreases as the jet angle increases beyond 90°. On the other hand, Figure 12 shows that changing the jet angle affects both the value of the maximum heat transfer at the step wall and its location. The change in the value of $h_{max}$ is small when the jet angle is less than 90, whereas, when $\theta$ increases more than 90, the values of $h_{max}$ drop drastically and the values of $X_m$ increases.

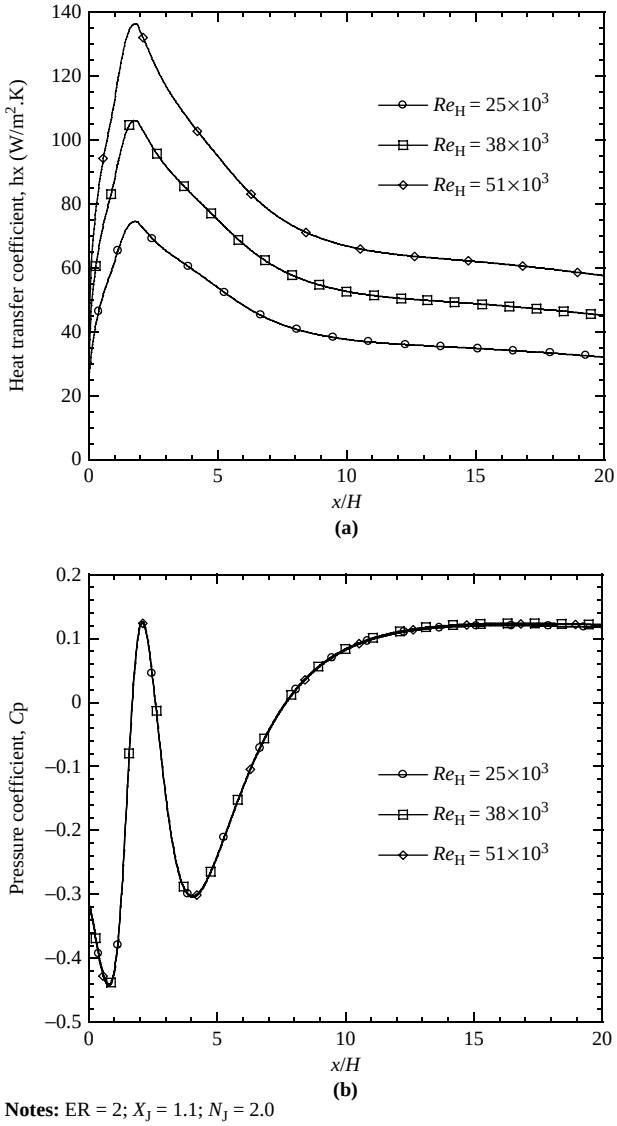


**Notes:** ER = 2; $X_J = 1.1$; $N_J = 2.0$

**Figure 10.**
The distribution of the: (a) heat transfer coefficient; and (b) pressure coefficient for different Reynolds numbers

| Jet location case | ER = 1.67 | | | ER = 1.8 | | | ER = 2.0 | | |
|---|---|---|---|---|---|---|---|---|---|
| | $X_m$ | $h_{max}$ | $X_r$ | $X_m$ | $h_{max}$ | $X_r$ | $X_m$ | $h_{max}$ | $X_r$ |
| J0 (no jet) | 4.55 | 66.60 | 5.91 | 4.64 | 65.52 | 6.15 | 4.50 | 65.18 | 6.10 |
| J3 | 3.30 | 88.12 | 3.32 | 3.32 | 90.35 | 3.28 | 3.46 | 93.54 | 3.32 |
| J7 | 8.08 | 74.46 | 5.42 | 8.14 | 76.78 | 5.67 | 8.14 | 80.51 | 5.94 |

**Notes:** $Re_H = 3.8 \times 10^4$; $\theta = 90°$

**Table II.**
Flow and heat transfer data obtained for different expansion ratios

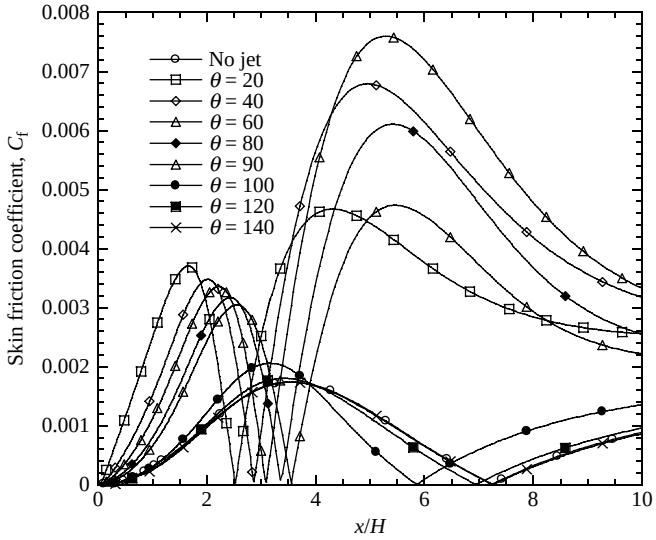


**Notes:** ER = 2; $X_J$ = 1.1; $N_J$ = 2.0; $Re_H = 3.8\times10^4$

**Figure 11.**
Distribution of the skin friction coefficient along the step wall at different jet angles

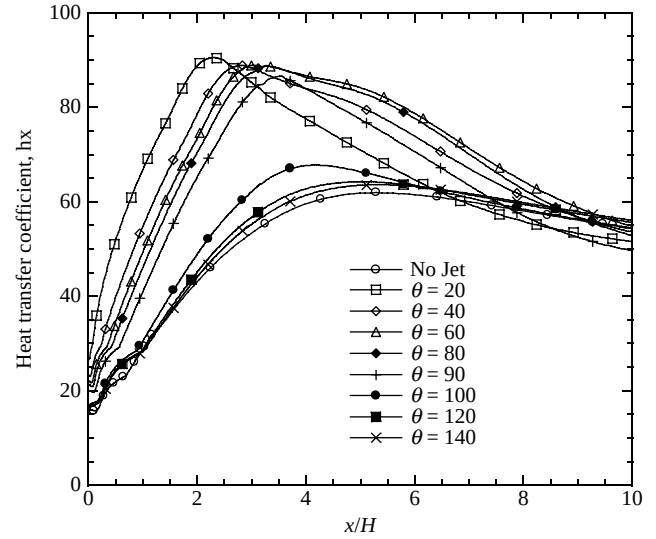


**Notes:** ER = 2; $X_J$ = 1.1; $N_J$ = 2.0; $Re_H = 3.8\times10^4$

**Figure 12.**
Distribution of the heat transfer coefficient along the step wall at different jet angles

The effect of jet angle on both flow and heat transfer characteristics can be understood by examining the effect of the size of the circulating bubble formed at jet wall. When $\theta$ is below 90°, the jet blows its fluid against the main stream and, therefore, the size of the circulating bubble at jet wall increases (Figure 13). Figure (13) also shows that as the jet angle increases, the size of this bubble decreases. When $\theta$ increases beyond 90°,

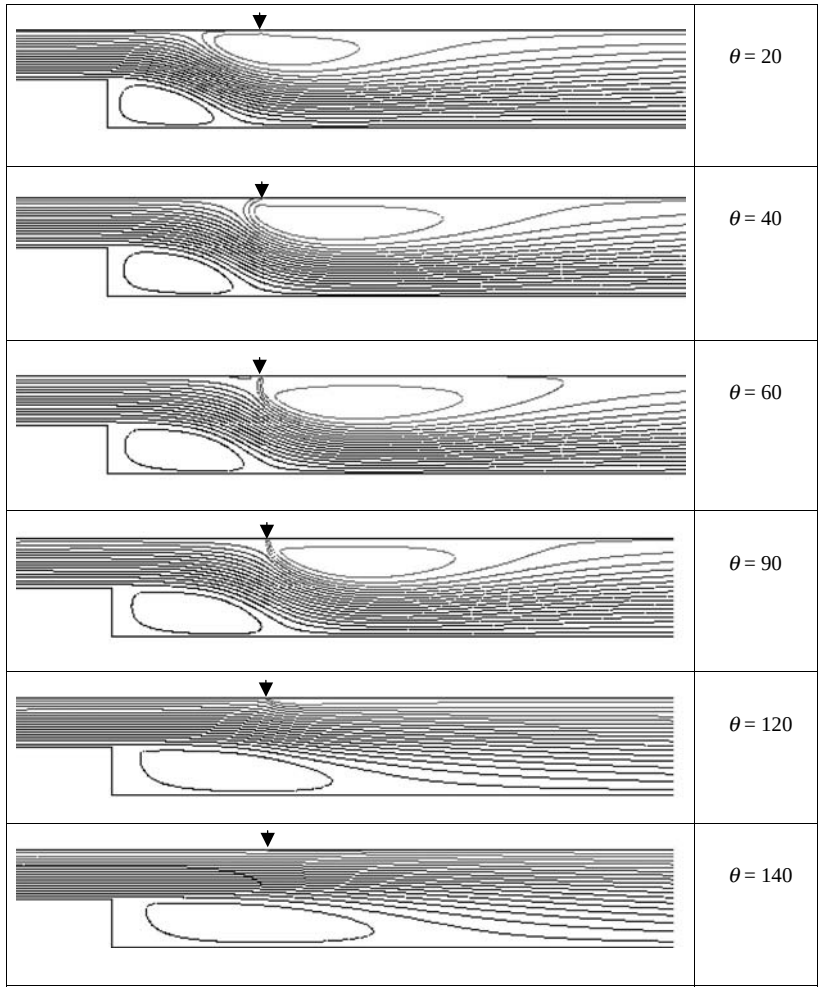


**Figure 13.**
Streamlines for selected jet angles

**Notes:** The arrow indicates the location of the jet $X_J = 3.1$; ER = 2; $Re_H = 3.8 \times 10^4$; Reproduced from the only available original

the jet blows its fluid along the main stream and therefore the size of this bubble decreases.

Figure 14 is shown in order to have a better insight into the effect of changing the jet angle on the flow field. The scale shown in the figure is common for all cases. The turbulent kinetic energy is mainly concentrated in the shear layer when no jet is applied. The application of the jet at angles below 90° diffuses the turbulence from the shear layer and increases its intensity in the recirculation region close to the step. This enhances heat transfer in that region. A substantial turbulence is generated in the wake of the jet. As the jet angle increases beyond 90° the turbulence in the shear layer is less affected by the presence of the jet.

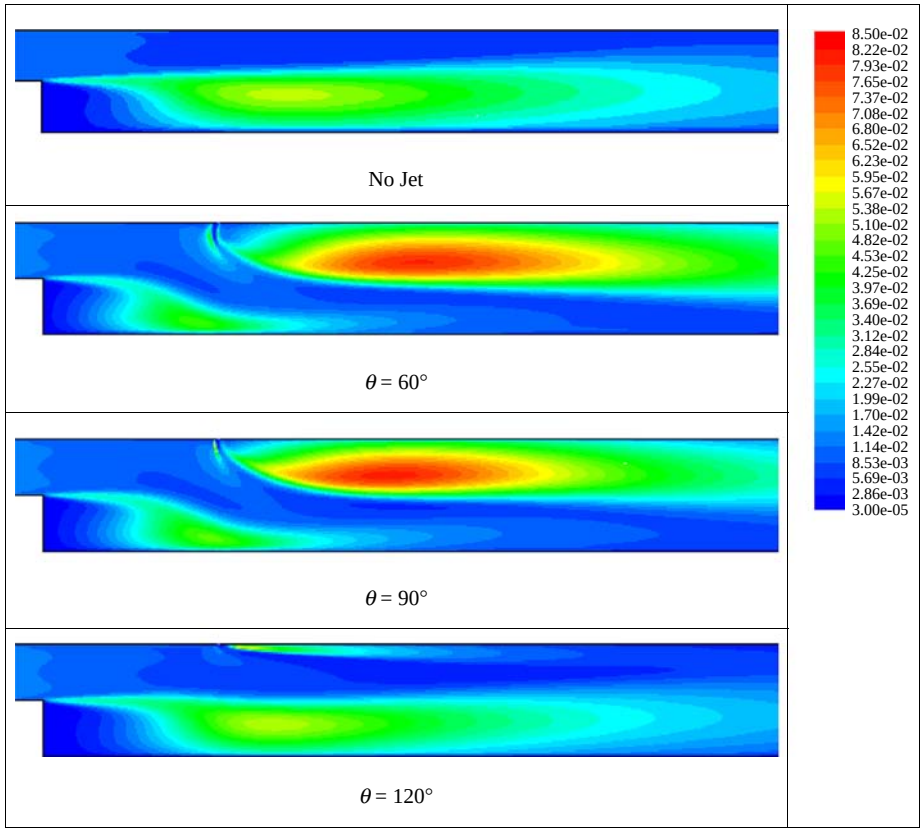


**Notes:** $X_J = 3.1$; ER = 2; $Re_H = 3.8 \times 10^4$

**Figure 14.**
Turbulent kinetic energy contours

## 5. Conclusions

The turbulent forced convection heat transfer of the flow over a backward facing step with the presence of jet opposing to the step wall is numerically investigated. The standard and the RNG $K - \varepsilon$ models are used. The effect of several parameters on the flow and heat transfer characteristics was investigated. These parameters include jet location, jet velocity, jet angle, expansion ratio, and Reynolds number. The main conclusions drawn from this work can be summarized as follows:

- Both the RNG and the standard $K - \varepsilon$ models have good ability to predict the reattachment length and the pressure coefficient. However, the RNG model over predicts the maximum heat transfer and its location.
- The use of a jet opposing to the step wall controls the size of the circulating bubble and therefore, the flow and heat transfer characteristics.
- The predictions obtained by the standard and the RNG $K - \varepsilon$ models when normalized by a reference case obtained by the same model agree with the experimental results normalized in the same manner.

- Locating the jet closer to the step reduces the size of the circulating bubble, reduces the reattachment length, and increases the heat transfer coefficient.
- Increasing the jet velocity at any location reduces the size of the circulating bubble and enhances heat transfer from the step wall.
- For the range of ER investigated in this work, increasing the expansion ratio has little effect on the heat transfer characteristics of the flow at all jet locations.
- Increasing Reynolds number of the flow increases the maximum heat transfer coefficient and has little influence on the reattachment length.
- Varying the jet angle controls the reattachment length over a wide range over the step wall.

## References

Abe, K., Kondoh, T. and Nagano, Y. (1995), "A new turbulence model for predicting fluid flow and heat transfer in separating and reattaching flows: II. Thermal field calculations", *Int. J. Heat Mass Transfer*, Vol. 38 No. 8, pp. 1467-81.

Abu-Hijleh, B.A.K. (2000), "Modifying reattaching shear layer using a rotating cylinder", *Computers & Fluids*, Vol. 29, pp. 261-73.

Avancha, R. and Pletcher, R. (2002), "Large eddy simulation of the turbulent flow past a backward facing step with heat transfer and property variation", *Int. J. of Heat and Fluid Flow*, Vol. 23 No. 5, pp. 601-14.

Barter, J. and Dolling, D. (1995), "Reduction of fluctuating pressure loads in shock boundary-layer interaction using vortex generators", *AIAA Journal*, Vol. 33 No. 10, pp. 1842-9.

Choudhury, D. (1993), "Introduction to the renormalization group method and turbulence modeling", Fluent Inc. Technical Memorandum TM-107.

Chyu, W., Rimlinger, M. and Shih, T. (1995), "Control of shock-wave/boundary-layer interactions by bleed", *AIAA Journal*, Vol. 33 No. 7, pp. 1239-47.

Debisschop, J. and Nieuwstat, F. (1996), "Turbulent boundary layer in an adverse pressure gradient: effectiveness of ripple", *AIAA Journal*, Vol. 34 No. 5, pp. 932-7.

Fluent (2001), *User's Guide*, Fluent Inc., Hanover, NH (Version 6.1.18).

Gad-el-Hak, M. and Bushnell, D. (1991), "Separation control: review", *Journal of Fluids Engineering*, Vol. 113, pp. 5-30.

Garsul, I., Srinivas, S. and Batta, G. (1995), "Active control of vortex breakdown over a delta wing", *AIAA Journal*, Vol. 33 No. 9, pp. 1734-6.

Hanna, R. (1995), "Hypersonic shockwave/turbulent boundary-layer interactions on a porous surface", *AIAA Journal*, Vol. 33 No. 10, pp. 1977-9.

Inaoka, K., Nakamura, K. and Senda, M. (2004), "Heat transfer control of a backward-facing step flow in a duct by means of miniature electromagnetic actuators", *Int. J. of Heat and Fluid Flow*, Vol. 25 No. 5, pp. 711-20.

Joslin, R., Nicolaides, R., Erlebacher, G., Hussaini, M. and Gunzburger, M. (1995), "Active control of boundary-layer instabilities: use of sensors and spectral controller", *AIAA Journal*, Vol. 33 No. 8, pp. 1521-3.

Kiwan, S. (1995), "Computations of a shear-driven three-dimensional turbulent boundary layer flow", PhD thesis, Department of MMAE, Illinois Institute of Technology, Chicago, IL.

Kral, L. and Fasel, H. (1994), "Direct numerical simulation of passive control of three-dimensional phenomena in boundary-layer transition using wall heating", *Journal of Fluid Mechanics*, Vol. 264, pp. 213-54.

Mohammadi, B. and Pironnean, O. (1993), *Analysis of the K-epsilon Turbulence Model*, Wiley, Chichester.

Nelson, C., Koga, D. and Eaton, J. (1990), "Unsteady separated flow behind an oscillating, two-dimensional spoiler", *AIAA Journal*, Vol. 28 No. 5, pp. 845-52.

Oyakawa, K., Shinzato, T. and Mabuti, I. (1986), "Effect on heat transfer augmentation of some geometric shapes of a turbulent promoter in a rectangular duct", *Bulletin of JSME*, Vol. 29, pp. 3415-20.

Oyakawa, K., Taira, T., Senaha, I., Nosoko, T. and Hiwada, M. (1995), "Heat transfer control by using jet discharge in reattachment region downstream of a backward facing step", *Int. Comm. of Heat and Mass Transfer*, Vol. 22 No. 3, pp. 343-52.

Roos, F. and Kegelman, J. (1986), "Control of coherent structures in reattaching laminar and turbulent shear layer", *AIAA Journal*, Vol. 24 No. 12, pp. 1956-63.

Suzuki, H., Kida, S., Nakamae, T. and Suzuki, K. (1991), "Flow and heat transfer over a backward-facing step with a cylinder mounted near its top corner", *Int. J. of Heat and Fluid Flow*, Vol. 12 No. 4, pp. 353-9.

Vakili, A. and Gauthier, C. (1994), "Control of cavity flow by upstream mass-injection", *Journal of Aircraft*, Vol. 30 No. 3, pp. 315-9.

Vogel, J. and Eaton, J. (1985), "Combined heat transfer and fluid dynamic measurements downstream of backward-facing step", *Tran. of ASME, J. of Heat Transfer*, Vol. 107, pp. 922-9.

Yakhot, V. and Orszag, S. (1986), "Renormalization group analysis of turbulence: I-basic theory", *Journal of Scientific Computing*, Vol. 1 No. 1, pp. 3-51.

Zhang, X. (1995), "Compressible cavity flow oscillation due to shear layer instability and pressure feedback", *AIAA Journal*, Vol. 33 No. 8, pp. 1404-11.

**Corresponding author**
Suhil Kiwan can be contacted at: kiwan@just.edu.jo